A recipe for desert : analysis of an extended Klausmeier model

Siero, E.P.J.A.

4 Effects of nonlocal grazing on dryland vegetation patterns

4.1 Introduction

Environmental stress, e.g. due to climate change or increased grazing, drives desertification. Annual mean precipitation is likely to decrease in many arid and semi-arid regions [87]. Contrary to climate change, grazing can in principle be managed locally and directly, which creates the opportunity to intervene. Timely measures that decrease the grazing pressure on ecosystems may help prevent regime shifts to a degraded bare desert state [149,163]. For this, expanding the understanding of grazing systems would be very useful.

A complexifying property of drylands is that spatially periodic vegetation patterns may emerge, even though the abiotic environment is (approximately) spatially homogeneous. The widespread occurrence of periodic vegetation patterns has been confirmed at the interface between arid and semi-arid regions [36]. A widely accepted pattern forming mechanism is the increased infiltration at vegetated soil (short range facilitation), in combination with overland redistribution of water during rain showers to the vegetated patches, where the soil conditions favor water infiltration (long range competition) [150]. This mechanism is present in many spatially extended arid ecosystem models, see e.g. [70, 79, 97, 148, 156].

Figure 4.1 shows a simulation of the desertification process in one space dimension x for one of these models, the extended Klausmeier model [97,180].[1] For large values of the rainfall a, the system resides in a stable homogeneously vegetated state. As rainfall decreases to a value below $a = 3$, the homogeneous state becomes Turing unstable [190]. A vegetation pattern forms with a certain wavelength, which remains the same for a range of a. Then a cascade of transitions to patterns with larger and larger wavelengths follows [180]. Finally, the system transitions from a large wavelength pattern

[1] With [180] corresponding to Chapter 2.

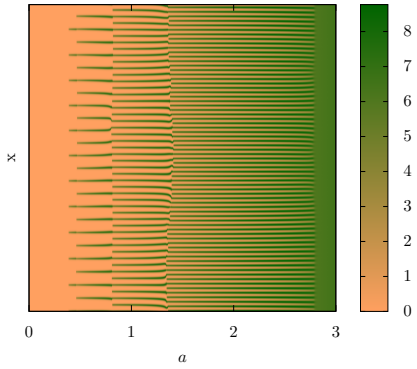

Figure 4.1: Desertification process driven by decreasing rainfall a ($\frac{da}{dt} = -10^{-4}$) in the absence of grazing, starting with a spatially homogeneous vegetation at $a = 3$, showing the evolution of the distribution of vegetation in a single space dimension x. The simulation is based on the extended Klausmeier model, see Section 4.5 for further details.

to the bare desert state and the desertification process is completed. This final transition is in accordance with (an extension of) one of Ni's conjectures [133]: the last patterns to destabilize have large wavelengths.

We aim to study the influence of grazing on this desertification process: on the pattern formation, pattern adaptation and the final transition to a bare desert state.

The most common way of incorporating senescence of vegetation n, in reaction-diffusion type arid ecosystem modeling, is by including a linear death term $-mn$, with m a constant parameter, see [70, 79, 97, 125, 135, 148, 156, 175, 202] among others. Occurrence of grazing has been viewed as included in the term $-mn$ [70, 125, 202], through a higher value of the coefficient m [156]. Here we analyze a refinement to this modeling by taking into account the nonlocal coupling grazing asserts on the vegetation [196]: the availability of (superior) forage elsewhere decreases foraging at a given location.

In Section 4.2 we account for the nonlocal coupling asserted by the grazing by combining the concepts of ideal free distribution [65], functional and numerical response [80, 181]. For this, plant death mn is split into the usual local linear term $m_0 n$ (non-grazing related senescence) and a nonlocal coupling for modeling grazing:

$$mn = m_0 n + \text{grazing}. \tag{4.1}$$

The grazing at any location will depend on the overall distribution of the vegetation. For this we assume that herbivore dynamics is fast compared to biomass evolution.

The ideal free distribution [65] is used to determine the spatial distribution of herbivores, which means that herbivores spread out such that the suitability of all locations is the same. There have been recent studies on (individual) herbivore foraging behavior in heterogeneous environments, see e.g. [31, 66] and the references therein, which extend this by also taking into account finite animal movement speed and incomplete knowledge of the resource distribution. We note that on the population level, all individual herbivores only need to comply with the ideal free distribution locally to enforce an ideal free distribution globally. We introduce a parameter j that models the preference of herbivores for the more vegetated locations.

The functional and numerical response [80, 181] of herbivores on available forage will be determined under simple assumptions both in the context of *sustained* grazing and *natural* grazing. In a system with sustained grazing we assume that the number of herbivores is kept constant, by always supplying supplementary food if necessary. For natural grazing we assume that supplementary food is never provided, so that herbivores need to completely sustain themselves. These cases are two extremes.

Section 4.3 incorporates the derived grazing terms in the two-component (surface water, plant biomass) extended Klausmeier model. This model has been used to study the desertification process driven by decreasing rainfall a both in one space dimension [180] and in two space dimensions [176][2], but in the absence of nonlocal coupling caused by grazing.

We restrict attention to sustained grazing with $j = 2$ and natural grazing with $j = 1$. These choices will allow for a direct comparison with the case without grazing, because the dependence on grazing of the homogeneously vegetated states themselves can in these cases be absorbed by the rainfall parameter.

In Section 4.4 we perform a linear stability analysis about the homogeneous steady state from where the desertification process starts, for the specific choices of grazing.

We show that for sufficiently severe sustained grazing with $j = 2$, the ho-

[2]With [176] corresponding to Chapter 3.

mogeneous steady state is destabilized by a Hopf instability before patterns form (at the Turing instability), which is in line with Result 1 below. In this case complete desertification is immediate and vegetation patterns are omitted. For natural grazing with $j = 1$ this is not the case: the homogeneous steady state generally becomes more susceptible to Turing instability as grazing becomes more severe.

Section 4.5 presents simulations for the same specific choices of grazing as in the previous section, all with decreasing rainfall as in Figure 4.1. For sustained grazing with $j = 2$ we perform a sequence of simulations with larger and larger numbers of herbivores, which increases the grazing pressure on all vegetation distributions proportionally. Not only do these simulations show that vegetation patterns can be suppressed (Result 1 below), but also that in the desertification process the large wavelength patterns are skipped (Result 2 below). For natural grazing with $j = 1$, the influence of increasing the grazing pressure on all vegetation distributions proportionally is studied with simulations. For this case we also vary herbivore persistence, which is herbivore ability to survive at low levels of available forage. The simulations show jumps from high to low forage states that become more dramatic if natural grazing is set to be more severe (Result 3 below).

Concerning grazing in the extended Klausmeier model, we have the following main results:

1. A strong preference of herbivores for locations with large available forage ($j > 1$) may suppress vegetation patterns altogether (as a manifestation of the tall poppy syndrome, Corollary 4.1 & Figure 4.6(d));
2. Sustained grazing impedes the existence of large wavelength patterns, causing a violation of Ni's conjecture (Figure 4.6, see also Section 4.6.1);
3. Natural grazing may create a dichotomy of high forage and low forage system states, with large respectively small numbers of herbivores. (Figure 4.8).

All these results likely hold for implementations of the derived grazing terms in other arid ecosystem models, as we discuss at the end of Section 4.2.

Result 1 has profound consequences for the desertification process, since in this case vegetation patterning will not always precede the transition to the bare desert state, so vegetation patterns are not an early warning signal

for complete land degradation. Result 2 means that, in case of a coarsening cascade of vegetation patterns, the penultimate state in the desertification process need not have a long wavelength; together with Result 3 it implies that

4. both sustained and natural grazing open up the possibility of a dramatic sudden regime shift [149, 163].

For sustained grazing the shift will be towards the bare desert state [196]. For natural grazing the regime shift will result in a low forage state.

We conclude that the proposed grazing model refinements dramatically alter the desertification process, but this alteration depends strongly on what model refinement is implemented.

Remark 4.1. *In this chapter we use as a domain a one-dimensional bounded interval with length L, though all ideas can be transported to two-dimensional or unbounded domains (by using an integration kernel for the grazing terms). As patterns in one space dimension correspond to banded vegetation in two space dimensions, we will refer to parts of the domain as areas.*

4.2 Modeling of grazing

In this section we develop nonlocal terms to model grazing. Modeling assumptions lead to Holling type II (sustained) and type III (natural) grazing response functions [80]. We model grazing by dissecting it in three parts and determining each part separately, as follows:

$$\text{grazing} = \text{spatial distribution} \times \text{functional response} \times \text{numerical response} \tag{4.2}$$

where we distinguish

- spatial distribution: spatial probability distribution of a single herbivore as a function of the distribution of the vegetation, assuming an ideal free distribution [65],
- functional response [80, 181]: consumption rate of a single herbivore as a function of available forage,
- numerical response [80, 181]: number of herbivores as a function of available forage.

Combining these concepts in this way is, as far as we know, a novel approach.

4.2.1 Ideal free distribution

An inhomogeneous distribution of biomass $n(x)$ leads to an inhomogeneous distribution of herbivores. Assuming that the system is in a steady state, we want to determine an ideal free distribution [65] of herbivores, which we express as the probability distribution of the location of a single herbivore. For this we need to make assumptions on the suitability S of a location. As the suitability is set to decrease with the density of herbivores, the ideal free distribution is attained if the suitability of all (occupied) locations is equal [65].

We set the suitability S of a location x to be solely determined by the effective foraging potential which we assume to be of the form $n^j(x)$ $(j > 0)$ divided by the herbivore density $\phi(x)$ among whom this forage is shared: $S(n, \phi) := n^j/\phi$. The ideal free distribution is attained if S is constant, so that the density of herbivores ϕ is proportional to n^j and the probability distribution of a single herbivore is given by

$$\frac{n^j(x)}{\int_0^L n^j(x)\ dx}, \tag{4.3}$$

where the denominator takes care of the normalization.

If $j = 1$, S is proportional to the local biomass. If only the amount of vegetation and not its spatial distribution affect total herbivory, then this is the natural choice for j.

Locations with large amounts of forage provide herbivores the opportunity to graze more efficiently, since it allows for a significant overlap of the searching and handling of forage [182]. Thus the attractivity of a vegetation patch may be superlinear in n, resulting in a suitability with $j > 1$. In this case a distribution of vegetation concentrated in patches can be grazed more than the same amount of biomass being smeared out equally over the whole domain.

If plants become less susceptible to herbivory as they grow [165], e.g. because of decreased palatability, then attractiveness of large vegetation patches may be less than proportional to the amount of biomass. This corresponds to a suitability with $0 < j < 1$. In this case a homogeneous distribution of vegetation will provide the most forage.

The effective forage potential of a vegetation distribution should reflect the (un)attractiveness of patches of vegetation, through the parameter j.

We define as *measures of forage* per unit area

$$I_j(n) := \frac{1}{L}\int_0^L n^j(x)\ dx, \tag{4.4}$$

with $j > 0$. Which measure of forage is relevant relates to the utilization and foraging behavior of the herbivores. From the subsequent derivation it will follow that the grazing rate ($= \frac{\text{grazing}}{n}$) is constant ('flat rate') if $j = 1$, so equal for densely and scarcely vegetated locations. A value $j > 1$ will make for a grazing rate that itself grows with increasing n ('progressive rate').

Substituting definition (4.4) into (4.3), the probability distribution of a single herbivore can be written as

$$\frac{n^j}{LI_j(n)}. \tag{4.5}$$

4.2.2 Sustained grazing

Although (for steady vegetation distributions) the spatial distribution of herbivores is constant on the population level, individual herbivores will still move around, so that the functional response of herbivores is affected by time spend moving and searching [64] (without handling [182]). Assuming that herbivores spend a fixed amount of time on foraging, the total individual forage of herbivores can be described by a Holling functional response type II [80]. For a system with sustained grazing, a constant effective herbivore number has been regarded as a good approximation of reality [134,196], any grazing deficiency will be compensated by supplementary food. We denote the imposed number of herbivores per unit area by h_{imp}.

From the previous discussion on sustained grazing we deduce two assumptions:

- the functional response is of type II;
- the numerical response is constant and equals $h_{\text{imp}}L$.

The functional response depends on the available forage, which is measured by $I_j(n)$ (4.4). For large $I_j(n)$, intake of the herbivores satiates at a maximal consumption rate $c_{\max}$. The type II functional response is given by

$$\frac{c_{\max}I_j(n)}{I_h + I_j(n)},$$

where I_h is the value of $I_j(n)$ where half of the maximum consumption rate is lost through searching.

Applying equation (4.2) with (4.5) in the setting with sustained grazing yields

$$\text{grazing} = \frac{n^j}{LI_j(n)} \times \frac{c_{\max} I_j(n)}{I_h + I_j(n)} \times h_{\text{imp}} L = \frac{m_{\text{sus}}}{I_h + I_j(n)} n^j \tag{4.6}$$

with $m_{\text{sus}} := c_{\max} h_{\text{imp}}$ the maximum rate of intake on the population level, per unit area.

The *total amount of grazing* for sustained grazing is given by

$$G_{j,\text{sus}}(n) := \int_0^L \frac{m_{\text{sus}}}{I_h + I_j(n)} n^j dx = \frac{m_{\text{sus}} L I_j(n)}{I_h + I_j(n)}. \tag{4.7}$$

The *grazing pressure*, defined as total intake $G_{j,\text{sus}}(n)$ divided by the total forage mass $LI_j(n)$ [2], is given by

$$g_{j,\text{sus}}(n) := \frac{G_{j,\text{sus}}(n)}{LI_j(n)} = \frac{m_{\text{sus}}}{I_h + I_j(n)}, \tag{4.8}$$

so that (4.6) can be concisely written as

$$\text{grazing} = g_{j,\text{sus}}(n) \cdot n^j. \tag{4.9}$$

4.2.3 Natural grazing

In a natural setting, given an amount of forage $I_j(n)$ (4.4), part of the herbivores will be able to sustain themselves by acquiring sufficient grazing intake for maintenance, e.g. by increasing foraging time. Other herbivores will disappear from the domain, e.g. due to death or emigration, relieving the remaining herbivores of high competition for suitable forage. Thus in this case the consumption of the remaining individuals is approximately constant at a sufficient sustenance level c_{suf}, but at the expense of a numerical response. As the available forage $I_j(n)$ decreases it may hardly be able to support any wildlife, even before all biomass has disappeared. At the other side of the spectrum where forage is abundant, the number of herbivores is assumed to be delimited by other factors, e.g. due to top-down control by predation.

We summarize this discussion on natural systems by listing two assumptions:

- the functional response is constant and equals c_{suf};

- the numerical response is sigmoid (corresponding to type III).

We model the numerical response by the sigmoid function

$$\frac{h_{\max} L I_j(n)^2}{{I_h}^2 + I_j(n)^2},$$

where I_h in this case represents the value of $I_j(n)$ where half of the maximal number of herbivores $h_{\max} L$ remain.

Applying equation (4.2) with (4.5) in the natural setting now yields

$$\text{grazing} = \frac{n^j}{L I_j(n)} \times c_{\text{suf}} \times \frac{h_{\max} L I_j(n)^2}{{I_h}^2 + I_j(n)^2} = \frac{m_{\text{nat}} I_j(n)}{{I_h}^2 + I_j(n)^2} n^j \tag{4.10}$$

with $m_{\text{nat}} := c_{\text{suf}} h_{\max}$ the maximum rate of intake on the population level, per unit area.

The *total grazing* is given by

$$G_{j,\text{nat}} := \int_0^L \frac{m_{\text{nat}} I_j(n)}{{I_h}^2 + I_j(n)^2} n^j dx = \frac{m_{\text{nat}} L I_j(n)^2}{{I_h}^2 + I_j(n)^2} \tag{4.11}$$

so that we identify the *grazing pressure* being

$$g_{j,\text{nat}}(n) := \frac{G_{j,\text{nat}}}{L I_j(n)} = \frac{m_{\text{nat}} I_j(n)}{{I_h}^2 + I_j(n)^2} \tag{4.12}$$

and (4.10) becomes

$$\text{grazing} = g_{j,\text{nat}}(n) \cdot n^j. \tag{4.13}$$

4.2.4 Comparison of sustained and natural grazing

We make a comparison of the total grazing (4.7), (4.11) and grazing pressure (4.9), (4.13) functions in the sustained and natural setting. In (4.14) the asymptotic behavior of the grazing functions is shown and we see that at $I_j(n) = I_h$ for both types of grazing intake is precisely half of the maximum intake on the population level.

	$G_{j,\text{sus}}$	$G_{j,\text{nat}}$	$g_{j,\text{sus}}$	$g_{j,\text{nat}}$
$I_j(n) \to 0$	$G_{j,\text{sus}} \to 0$	$G_{j,\text{nat}} \to 0$	$g_{j,\text{sus}} \to \frac{m_{\text{sus}}}{I_h}$	$g_{j,\text{nat}} \to 0$
$I_j(n) = I_h$	$G_{j,\text{sus}} = \frac{m_{\text{sus}} L}{2}$	$G_{j,\text{nat}} = \frac{m_{\text{nat}} L}{2}$	$g_{j,\text{sus}} = \frac{m_{\text{sus}}}{2 I_h}$	$g_{j,\text{nat}} = \frac{m_{\text{nat}}}{2 I_h}$
$I_j(n) \to \infty$	$G_{j,\text{sus}} \to m_{\text{sus}} L$	$G_{j,\text{nat}} \to m_{\text{nat}} L$	$g_{j,\text{sus}} \to 0$	$g_{j,\text{nat}} \to 0$

(4.14)

Regardless the setting, in a regime of abundant vegetation total grazing converges to the maximal overall intake rate mL and grazing pressure diminishes. Also, as available forage $I_j(n)$ becomes smaller but $I_j(n) > I_h$, the grazing pressure monotonically increases. The main difference between the sustained and natural setting occurs when $I_j(n)$ decreases below I_h, since then in the sustained setting grazing pressure increases more and more (due to constant herbivore numbers, with a type II functional response) whereas in the natural setting herbivore numbers start reducing so fast (sigmoid response) that the grazing pressure starts to become smaller again from $I_j(n)$ below I_h onward. This is reflected by the sigmoid form of the total grazing $G_{j,\mathrm{nat}}$, see Figure 4.2.

Remark 4.2. *Since the sustained and natural grazing functions (with* $m_{\mathrm{sus}} = m_{\mathrm{nat}}$ *and the same value of* j*) are almost equal for* $I_j(n) \gg I_h$*, in this regime the same dynamics are likely to occur for sustained and natural grazing.*

With the proposed grazing functions set, we return to the main results of the introduction to see how they fit.

1. The grazing rate ($= \frac{\text{grazing}}{n} = g_j n^{j-1}$) is an increasing function of n for $j > 1$ ('progressive'), so that locations with relatively large biomass bear a large grazing rate and locations with small biomass bear a small grazing rate. If this difference is large enough, this may lead to levelling out of vegetation distributions resulting in a spatially homogeneous vegetation.
2. For sustained grazing, periodic vegetation patterns with large wavelength have low available forage $I_j(n)$ and thus are subjected to a large grazing pressure, see Figure 4.2(b).
3. For natural grazing, states with intermediate amounts of forage $I_j(n) = I_h$ experience the heighest levels of grazing pressure, Figure 4.2(b). A small I_h corresponds to persistent herbivores, so the available forage $I_j(n)$ of possibly inadmissible states is influenced by herbivore persistence, creating a dichotomy of higher forage and lower forage states.

4.3 Incorporation of grazing in the extended Klausmeier model

As announced in the introduction, we analyze the proposed nonlocal grazing terms within an extended Klausmeier model [176, 180]. On flat ground, in

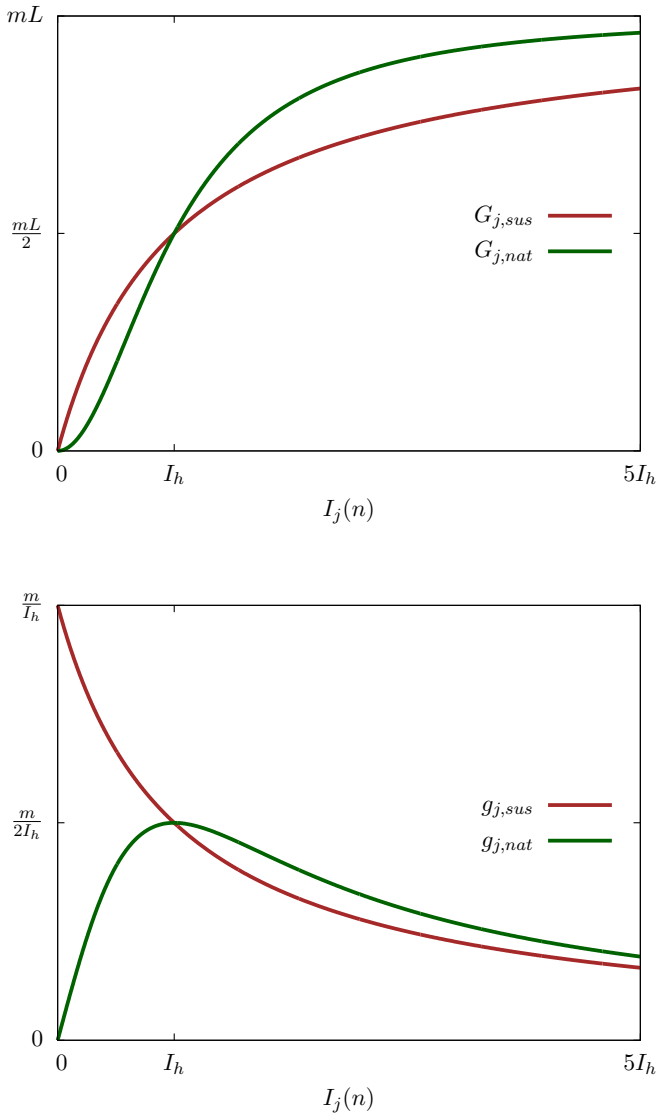

Figure 4.2: Grazing as a function of available forage $I_j(n)$. Here I_h designates the amount of forage where the total grazing is half the maximum value and $m = m_{\text{sus}}$ or m_{nat} respectively. Note that the graphs do not depend on j. Top panel: in both cases the total grazing G converges to mL as forage becomes more and more abundant and diminishes if vegetation becomes scarce. Bottom panel: in both cases the grazing pressure g is (approximately) inversely proportional to available forage in case of abundant forage. The function $g_{j,\text{sus}}$ monotonically increases to m/I_h as all vegetation disappears; in contrast $g_{j,\text{nat}}$ initially increases to a maximum at $I_j(n) = I_h$ but then converges to zero for ever smaller forage amount.

dimensionless form, it is given by

$$\begin{aligned} w_t =& d_1 w_{xx} + f(w,n), \\ n_t =& d_2 n_{xx} + g(w,n) \end{aligned} \tag{4.15}$$

where the reaction terms are given by

$$\begin{aligned} f(w,n) =& a - w - wn^2, \\ g(w,n) =& -mn + wn^2. \end{aligned} \tag{4.16}$$

As mentioned in the introduction, we choose a finite but large domain $[0, L]$, with Neumann or periodic boundary conditions. The second order derivatives w_{xx} and n_{xx} model water diffusion and plant dispersal, with water diffusion being faster so $d_1 \gg d_2$ (although in the original Klaumeier model [97], extensively analyzed in [173] and references therein, it holds that $d_1 = 0$). The parameter $a \geq 0$ models rainfall and may change as a function of time due to a changing climate; $-w$ models evaporation, m is an effective death rate and the terms $\pm wn^2$ model water uptake by the vegetation.

Remark 4.3. *When having to fix parameters, we do so in accordance with those employed in previous studies [97, 176, 180]:* $d_1 = 500$, $d_2 = 1$ *and* $m_0 = 0.45$.

As discussed in the introduction we now restrict to certain types of grazing that allow for a straightforward comparison with the case without grazing. Specifically, we choose $I_h = 1$ and sustained grazing with $j = 2$ or natural grazing with $j = 1$. It is of notational convenience that we now treat both types of grazing at once, we assume that either one has been set to zero. The realization of (4.1) with (4.9) and (4.13) is

$$\begin{aligned} mn =& m_0 n + g_{2,\mathrm{sus}}(n) \cdot n^2 + g_{1,\mathrm{nat}}(n) \cdot n \\ =& m_0 n + \frac{m_{\mathrm{sus}}}{1 + I_2(n)} n^2 + \frac{m_{\mathrm{nat}} I_1(n)}{1 + (I_1(n))^2} n \end{aligned} \tag{4.17}$$

where $m_0 > 0$, $m_{\mathrm{sus}}, m_{\mathrm{nat}} \geq 0$ (and $m_{\mathrm{sus}} m_{\mathrm{nat}} = 0$). By substituting (4.17) in (4.16), grazing is incorporated in the extended Klausmeier model.

4.4 Linear analysis of pattern formation with grazing

The grazing terms can alter both the homogeneous steady state solutions and their stability. In Section 4.3 we have restricted our attention to choices

for which the effect on the homogeneous steady states can be absorbed in the rainfall parameter, as we show in Section 4.4.1.

Next we focus on stability of the homogeneous steady states. Through a linear stability analysis, we identify possible scenarios for destabilization of a homogeneously vegetated state in the presence of grazing, which could result in vegetation pattern formation but could also lead to immediate desertification.

4.4.1 Homogeneous steady states

As in previous papers [176,180], when looking for homogeneous steady states we set $f(w,n) = g(w,n) = 0$ (see (4.16)) and obtain:

$$\begin{aligned} a - w - wn^2 &= 0, \\ -mn + wn^2 &= 0. \end{aligned}$$

One solution is given by $n_{\text{bare}} = 0$ and consequently $w_{\text{bare}} = a$, which corresponds to the bare desert state.

Otherwise

$$\begin{aligned} m &= wn, \\ w &= \frac{a}{1+n^2} \end{aligned} \tag{4.18}$$

so that

$$m = \frac{an}{1+n^2}. \tag{4.19}$$

Because $I_1(n) = n$ and $I_2(n) = n^2$, (4.17) simplifies to

$$m = m_0 + \frac{m_{\text{sus}} + m_{\text{nat}}}{1+n^2} n. \tag{4.20}$$

Substituting this into (4.19) we obtain

$$m_0 = \frac{(a - m_{\text{sus}} - m_{\text{nat}})n}{1+n^2}.$$

Setting $\bar{a} := a - m_{\text{sus}} - m_{\text{nat}}$ this leads to

$$m_0(1+n^2) = \bar{a}n \tag{4.21}$$

which is a quadratic equation in n having solutions

$$n_{\pm}(\bar{a}, m_0) = \frac{\bar{a} \pm \sqrt{\bar{a}^2 - 4m_0^2}}{2m_0} \qquad (\bar{a} \geq 2m_0). \tag{4.22}$$

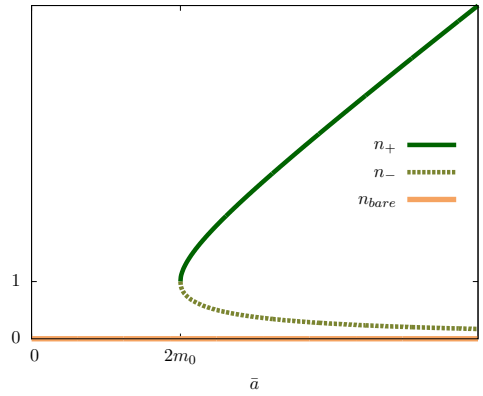

Figure 4.3: Homogeneous steady states of the extended Klausmeier model. For sustained grazing with $j = 2$ or natural grazing with $j = 1$, the grazing is absorbed into the rainfall a, together $\bar{a}$. In this case, the homogeneous steady states depend on $\bar{a}$ identically as they depend on a in the case without grazing ([180], Figure 2.8).

This shows that a fold or saddle-node bifurcation occurs at

$$\bar{a} = 2m_0, \tag{4.23}$$

or $a = 2m_0 + m_{\text{sus}} + m_{\text{nat}}$. The other component $w_\pm$ can be computed from (4.22) and any of the equations (4.18).

Remark 4.4. *We started out with independent parameters $a, m_0, m_{\text{sus}}, m_{\text{nat}}$ and introduced $\bar{a}$ as a dependent parameter. Since $n_\pm$ only directly depends on $\bar{a}$ and m_0, for the continuation of this section it will be easier to view $\bar{a}$ as an independent parameter and have a depend on $\bar{a}, m_{\text{sus}}, m_{\text{nat}}$.*

Remark 4.5. *The choice of $I_h = 1$ and the restriction to sustained grazing with $j = 2$ and natural grazing with $j = 1$ means that when $I_2(n)$ respectively $I_1(n)$ has decreased to 1, the total sustained grazing $G_{2,\text{sus}}$ respectively total natural grazing $G_{1,\text{nat}}$ have decreased to half the maximum total grazing. If destabilization of (w_+, n_+) for sustained grazing with $j = 2$ occurs for $n_+^2 = I_2(n_+) \gg 1$, then this likely also occurs for natural grazing, see Remark 4.2. Vice versa if (w_+, n_+) destabilizes for natural grazing with $j = 1$ when $n_+ = I_1(n_+) \gg 1$, then this likely also occurs for sustained grazing.*

4.4.2 Linearization of kinetics about $(w_\pm, n_\pm)$

We compute the linearization of the reaction terms about the homogeneous steady states $(w_\pm, n_\pm)$. To reduce notational burden, we abbreviate $(w_\pm, n_\pm)$ by (w, n) since we now only focus on these system states. As notation for the derivatives we introduce

$$\begin{aligned} a_1 :=& \frac{\partial f}{\partial w}(w,n) = -1 - n^2, \\ a_2 :=& \frac{\partial f}{\partial n}(w,n) = -2wn, \\ a_3 :=& \frac{\partial g}{\partial w}(w,n) = n^2, \\ a_4 :=& \frac{\partial g}{\partial n}(w,n) = -\frac{\partial (m(n)n)}{\partial n} + 2wn. \end{aligned} \tag{4.24}$$

We note that a_1 and a_3 only depend on n. We view $n_\pm(\bar{a}, m_0)$ as independent of m_{sus} and m_{nat}, see Remark 4.4. This also makes a_1 and a_3 independent of these parameters. The function a_2 does depend on m_{sus} and m_{nat} through w. By (4.16) and (4.17), $g(w,n) = -m_0 n - g_{2,\text{sus}}(n)\cdot n^2 - g_{1,\text{nat}}(n)\cdot n + wn^2$, so

$$\begin{aligned} a_4 =& -m_0 - \frac{\partial g_{2,\text{sus}}(n)}{\partial n} n^2 - \frac{2m_{\text{sus}} n}{1+n^2} - \frac{\partial g_{1,\text{nat}}(n)}{\partial n} n - \frac{m_{\text{nat}} n}{1+n^2} + 2wn \\ =& m_0 - \frac{\partial g_{2,\text{sus}}(n)}{\partial n} n^2 - \frac{\partial g_{1,\text{nat}}(n)}{\partial n} n + \frac{m_{\text{nat}} n}{1+n^2} \end{aligned} \tag{4.25}$$

where we used (4.18) and (4.20). Since $g_{2,\text{sus}}$ and $g_{1,\text{nat}}$ contain integrals, their differentation requires a bit more attention, for this we rely on outcomes of the more general linearization computations in Appendix 4.A.

Given a perturbation $(\tilde{w}(x), \tilde{n}(x))$ we may split it in a homogeneous and inhomogeneous part:

$$\begin{aligned} (\tilde{w}, \tilde{n})_{\text{hom}} :=& \left(\int_0^L \tilde{w}\ dx, \int_0^L \tilde{n}\ dx \right), \\ (\tilde{w}, \tilde{n})_{\text{inh}} :=& (\tilde{w}, \tilde{n}) - (\tilde{w}, \tilde{n})_{\text{hom}}. \end{aligned}$$

For the inhomogeneous part it follows from (4.25), (4.A.5) and (4.A.6), since $\beta_0 = 0$, that

$$a_{4,\text{inh}} = m_0 + \frac{m_{\text{nat}} n}{1+n^2}, \tag{4.26}$$

which does not depend on m_{sus}. For spatially homogeneous perturbations, it follows that

$$\begin{aligned} a_{4,\text{hom}} =& m_0 - \frac{-m_{\text{sus}}}{(1+n^2)^2} \cdot 2n \cdot n^2 - m_{\text{nat}} \frac{1-n^2}{(1+n^2)^2} n + \frac{m_{\text{nat}} n}{1+n^2} \\ =& m_0 + \frac{2(m_{\text{sus}} + m_{\text{nat}}) n^3}{(1+n^2)^2}. \end{aligned}$$

For the stability against homogeneous perturbations,

$$A_{\text{hom}} := \begin{pmatrix} a_1 & a_2 \\ a_3 & a_{4,\text{hom}} \end{pmatrix} = \begin{pmatrix} -1-n^2 & -2m_0 - \frac{2(m_{\text{sus}}+m_{\text{nat}})n}{1+n^2} \\ n^2 & m_0 + \frac{2(m_{\text{sus}}+m_{\text{nat}})n^3}{(1+n^2)^2} \end{pmatrix}$$

is relevant. We calculate the determinant

$$\begin{aligned} \det(A_{\text{hom}}) =& a_1 a_{4,\text{hom}} - a_2 a_3 \\ =& (-1-n^2) \left(m_0 + \frac{2(m_{\text{sus}} + m_{\text{nat}}) n^3}{(1+n^2)^2} \right) \\ & + \left(2m_0 + \frac{2(m_{\text{sus}} + m_{\text{nat}}) n}{1+n^2} \right) n^2 \\ =& m_0 (n^2 - 1) \end{aligned}$$

which does not depend on m_{sus} and m_{nat} (since n only depends on $\bar{a}$ and m_0, Remark 4.4). We note that $n_- < 1$ so then $\det(A_{\text{hom}}) < 0$, so (w_-, n_-) is unstable. On the other hand $n_+ > 1$ implies $\det(A_{\text{hom}}) > 0$, so that stability of (w_+, n_+) against homogeneous perturbations depends on the sign of the trace, where a change in sign signals a Hopf instability. From now on we focus on (w_+, n_+).

4.4.3 Hopf instability of (w_+, n_+)

Here (w, n) denotes (w_+, n_+). It holds that

$$\begin{aligned} \operatorname{tr}(A_{\text{hom}}) =& a_1 + a_{4,\text{hom}} \\ =& -(1+n^2) + m_0 + \frac{2(m_{\text{sus}} + m_{\text{nat}}) n^3}{(1+n^2)^2} \end{aligned} \tag{4.27}$$

which by equation (4.21) becomes

$$\operatorname{tr}(A_{\text{hom}}) = -\frac{\bar{a} n}{m_0} + m_0 + \frac{2(m_{\text{sus}} + m_{\text{nat}}) m_0^2 n}{\bar{a}^2}. \tag{4.28}$$

At the Hopf instability threshold it holds that $\mathrm{tr}(A_{\mathrm{hom}}) = 0$, so

$$\left(\bar{a}^3 - 2m_0^3(m_{\mathrm{sus}} + m_{\mathrm{nat}})\right) n = m_0^2 \bar{a}^2. \tag{4.29}$$

We compute $\mathrm{tr}(A_{\mathrm{hom}})$ on the fold bifurcation, where $\bar{a} = 2m_0$ (by (4.23)) and $n = 1$. Inserting this in (4.28) yields

$$\begin{aligned} \mathrm{tr}(A_{\mathrm{hom}}) = &-2 + m_0 + \frac{1}{2}(m_{\mathrm{sus}} + m_{\mathrm{nat}}) \\ &\begin{cases} < 0 & \text{if } m_0 < 2 - \frac{1}{2}(m_{\mathrm{sus}} + m_{\mathrm{nat}}) \qquad \text{(Hopf stable)} \\ > 0 & \text{if } m_0 > 2 - \frac{1}{2}(m_{\mathrm{sus}} + m_{\mathrm{nat}}) \qquad \text{(Hopf unstable)} \end{cases} \end{aligned} \tag{4.30}$$

so the Hopf instability locus on the fold moves to smaller values of m_0 for increasing m_{sus} or m_{nat}, and exists only for $m_{\mathrm{sus}} + m_{\mathrm{nat}} < 4$ (since $m_0 > 0$).

Since $\lim_{\bar{a}\to\infty} n = \infty$ but $n < \frac{\bar{a}}{m_0}$, it holds that for fixed $m_0 > 0$ and $m_{\mathrm{sus}}, m_{\mathrm{nat}} \geq 0$

$$\lim_{\bar{a}\to\infty} \mathrm{tr}(A_{\mathrm{hom}}) = -\infty. \tag{4.31}$$

Lemma 4.1 (Hopf curve monotonicity)**.** *No Hopf instabilities exist for triplets $(m_0, m_{\mathrm{sus}}, m_{\mathrm{nat}})$ with $m_0 < 2 - \frac{1}{2}(m_{\mathrm{sus}} + m_{\mathrm{nat}})$. For triplets with $m_0 \geq \max\left\{0, 2 - \frac{1}{2}(m_{\mathrm{sus}} + m_{\mathrm{nat}})\right\}$, there exists a unique Hopf instability; it moves to higher values of $\bar{a}$ for increasing m_0, m_{sus} or m_{nat}.*

Proof. Dividing (4.29) by $\bar{a}^2$ we obtain

$$\frac{\bar{a}^3 - 2m_0^3(m_{\mathrm{sus}} + m_{\mathrm{nat}})}{\bar{a}^2} n = m_0^2. \tag{4.32}$$

Define

$$\begin{aligned} D_- &:= \left\{(\bar{a}, m_0, m_{\mathrm{sus}}, m_{\mathrm{nat}}) : \bar{a}^2 - 2m_0^3(m_{\mathrm{sus}} + m_{\mathrm{nat}}) \leq 0\right\}, \\ D_+ &:= \left\{(\bar{a}, m_0, m_{\mathrm{sus}}, m_{\mathrm{nat}}) : \bar{a}^2 - 2m_0^3(m_{\mathrm{sus}} + m_{\mathrm{nat}}) > 0\right\}. \end{aligned}$$

Since the right-hand side of (4.32) is positive, it can't have solutions on D_-, so we restrict attention to D_+.

On D_+ the left-hand side is a monotonically increasing function of $\bar{a}$ and the right-hand side is independent of $\bar{a}$, so that for each combination $m_0 > 0$, $m_{\mathrm{sus}}, m_{\mathrm{nat}} \geq 0$ there can be at most one Hopf instability. By (4.30) and (4.31) a unique Hopf instability exists only for $m_0 > 2 - \frac{1}{2}(m_{\mathrm{sus}} + m_{\mathrm{nat}})$ (and $m_0 > 0$).

On D_+, for each fixed $\bar{a}$, the left-hand side is a decreasing function of m_0, m_{sus} and m_{nat}, since n is a decreasing function of m_0 for each fixed $\bar{a}$. The right-hand side is a non-decreasing function of m_0, m_{sus} and m_{nat}. So the Hopf instability moves to a higher value of $\bar{a}$ for larger m_0, m_{sus} or m_{nat}.

□

Since m_{sus} and m_{nat} are interchangeable in (4.28), (w, n) becomes equally more susceptible to Hopf instability in case of increased sustained grazing with $j = 2$ or increased natural grazing with $j = 1$. The Hopf instabilities for various values of $m_{\text{sus}}, m_{\text{nat}}$ for a realistic choice of parameters are plotted in Figure 4.4, illustrating that the Hopf instability curve moves to larger $\bar{a}$ for increasing m_{sus} or m_{nat}.

4.4.4 Turing instability of (w_+, n_+)

We again denote (w_+, n_+) by (w, n). Regarding a possible Turing instability we look at spatially inhomogeneous perturbations, with linearization given by

$$\begin{aligned} A_{\text{inh}}(\bar{a}, m_0, m_{\text{sus}}, m_{\text{nat}}) &:= \begin{pmatrix} a_1 & a_2 \\ a_3 & a_{4,\text{inh}} \end{pmatrix} \\ &= \begin{pmatrix} -1-n^2 & -2m_0 - \frac{2(m_{\text{sus}}+m_{\text{nat}})n}{1+n^2} \\ n^2 & m_0 + \frac{m_{\text{nat}}n}{1+n^2} \end{pmatrix}, \end{aligned} \tag{4.33}$$

see (4.24) and (4.26). We compute

$$\begin{aligned} \det(A_{\text{inh}}) =& a_1 a_{4,\text{inh}} - a_2 a_3 \\ =& (-1-n^2)\left(m_0 + \frac{m_{\text{nat}}n}{1+n^2}\right) + \left(2m_0 + 2n\frac{m_{\text{sus}}+m_{\text{nat}}}{1+n^2}\right)n^2 \\ =& (n^2-1)m_0 + \frac{-m_{\text{nat}}n - m_{\text{nat}}n^3 + 2n^3(m_{\text{sus}}+m_{\text{nat}})}{1+n^2} \\ =& (n^2-1)m_0 + \frac{2m_{\text{sus}}n^3 + m_{\text{nat}}n(n^2-1)}{1+n^2} > 0 \end{aligned}$$

and define

$$\text{Tur}(\bar{a}, m_0, m_{\text{sus}}, m_{\text{nat}}) := \Gamma - 2\sqrt{d_1 d_2 \det(A_{\text{inh}})}, \tag{4.34}$$

where $\Gamma := d_1 a_{4,\text{inh}} + d_2 a_1$, with d_1 and d_2 the diffusion constants.

The homogeneous steady state is Turing unstable if Tur > 0 and Turing stable if Tur < 0, see [176]. Note that these results follow from analysis of the continuous spectrum that relates to unbounded domains, in case of a (large) finite domain the instability is delayed (by a negligible amount).

Like for the Hopf instability we investigate Turing (in)stability on the fold bifurcation, where $\bar{a} = 2m_0$ (4.23) and $n = 1$. Substitution in (4.34) yields

$$\begin{aligned}\text{Tur} =& d_1\left(m_0 + \frac{m_{\text{nat}}}{2}\right) - 2d_2 - 2\sqrt{d_1 d_2 m_{\text{sus}}} \\ &\begin{cases} < 0 & \text{if } m_0 < 2\frac{d_2}{d_1} + 2\sqrt{\frac{d_2}{d_1}m_{\text{sus}}} - \frac{m_{\text{nat}}}{2} \qquad \text{(Turing stable)} \\ > 0 & \text{if } m_0 > 2\frac{d_2}{d_1} + 2\sqrt{\frac{d_2}{d_1}m_{\text{sus}}} - \frac{m_{\text{nat}}}{2} \qquad \text{(Turing unstable).} \end{cases}\end{aligned} \tag{4.35}$$

Lemma 4.2 (Turing curve monotonicity)**.** *No Turing instabilities exist for triplets* $(m_0, m_{\text{sus}}, m_{\text{nat}})$ *with* $m_0 < 2\frac{d_2}{d_1} + 2\sqrt{\frac{d_2}{d_1}m_{\text{sus}}} - \frac{m_{\text{nat}}}{2}$*. For triplets* $(m_0, m_{\text{sus}}, m_{\text{nat}})$ *with* $m_0 \geq \max\left\{2\frac{d_2}{d_1} + 2\sqrt{\frac{d_2}{d_1}m_{\text{sus}}} - \frac{m_{\text{nat}}}{2}\right\}$ *there exists a unique Turing instability; it moves to higher values of* $\bar{a}$ *for increasing* m_0*.*

Proof. This monotonicity was already shown in [176] in the absence of nonlocal grazing terms ($m_{\text{sus}} = m_{\text{nat}} = 0$), we will apply the framework provided there to also apply it to the cases with grazing. It is sufficient to show that

$$\operatorname{sgn}\frac{\partial a_1}{\partial \bar{a}} = \operatorname{sgn}\frac{\partial a_{4,\text{inh}}}{\partial \bar{a}} = \operatorname{sgn}\left(-\frac{\partial \det(A_{\text{inh}})}{\partial \bar{a}}\right) = -1$$

which means that increasing $\bar{a}$ acts stabilizing and

$$\operatorname{sgn}\frac{\partial a_1}{\partial m_0} = \operatorname{sgn}\frac{\partial a_{4,\text{inh}}}{\partial m_0} = \operatorname{sgn}\left(-\frac{\partial \det(A_{\text{inh}})}{\partial m_0}\right) = 1$$

which means that increasing m_0 acts destabilizing.

Since a_1 is unaffected by the grazing terms, we only compute

$$\begin{aligned}
\frac{\partial a_{4,\mathrm{inh}}}{\partial \bar{a}} =& m_{\mathrm{nat}} \frac{1-n^2}{(1+n^2)^2} \frac{\partial n}{\partial \bar{a}} < 0 \\
\frac{\partial a_{4,\mathrm{inh}}}{\partial m_0} =& 1 + m_{\mathrm{nat}} \frac{1-n^2}{(1+n^2)^2} \frac{\partial n}{\partial m_0} > 0 \\
\frac{\partial \det(A_{\mathrm{inh}})}{\partial \bar{a}} =& 2m_0 n \frac{\partial n}{\partial \bar{a}} + \frac{m_{\mathrm{sus}}\left(n^4+6n^2\right) + m_{\mathrm{nat}}\left(n^4+3n^2-1\right)}{(1+n^2)^2} \frac{\partial n}{\partial \bar{a}} > 0 \\
\frac{\partial \det(A_{\mathrm{inh}})}{\partial m_0} =& 2m_0 n \frac{\partial n}{\partial m_0} + n^2 - 1 \\
&+ \frac{m_{\mathrm{sus}}\left(n^4+6n^2\right) + m_{\mathrm{nat}}\left(n^4+3n^2-1\right)}{(1+n^2)^2} \frac{\partial n}{\partial m_0} < 0
\end{aligned}$$

where the final estimate follows from the estimate $\frac{\partial n}{\partial m_0} \leq -\frac{a}{m_0^2}$ as in [176].

Since for $m_0 < 2\frac{d_2}{d_1} + 2\sqrt{\frac{d_2}{d_1} m_{\mathrm{sus}}} - \frac{m_{\mathrm{nat}}}{2}$, (w, n) was already Turing stable on the fold $\bar{a} = 2m_0$, it remains stable for all $\bar{a} > 2m_0$. The linear results on pattern formation from [176] apply, in particular that for fixed $m_{\mathrm{sus}}, m_{\mathrm{nat}} \geq 0$ and $m_0 \geq 2\frac{d_2}{d_1} + 2\sqrt{\frac{d_2}{d_1} m_{\mathrm{sus}}} - \frac{m_{\mathrm{nat}}}{2}$, the unique $\bar{a}$-value of the Turing instability locus monotonically increases as m_0 increases. □

Sustained grazing with $j = 2$

The previous result Lemma 4.2 automatically leads to the simple consequence that a desertification process without Turing patterns is promoted by increasing m_{sus}.

Corollary 4.1. *Let $m_{\mathrm{nat}} = 0$ and m_{sus} be fixed. If*

$$m_0 < 2\frac{d_2}{d_1} + 2\sqrt{\frac{d_2}{d_1} m_{\mathrm{sus}}},$$

then (w, n) doesn't become Turing unstable as $\bar{a}$ decreases.

We now study further how sustained grazing with $j = 2$ affects the Turing instability. We do some preparatory work. First we compute the componentwise derivative of A_{inh} (4.33) with respect to m_{sus}:

$$\frac{\partial A_{\mathrm{inh}}}{\partial m_{\mathrm{sus}}} = \begin{pmatrix} 0 & \frac{-2n}{1+n^2} \\ 0 & 0 \end{pmatrix} \tag{4.36}$$

Now the first and second derivatives of Tur against any $m_\bullet$, be it m_{sus} or m_{nat}, are given by

$$\frac{\partial \text{Tur}}{\partial m_\bullet} = \frac{\partial \Gamma}{\partial m_\bullet} - \sqrt{\frac{d_1 d_2}{\det(A_{\text{inh}})}} \frac{\partial \det(A_{\text{inh}})}{\partial m_\bullet}, \tag{4.37}$$

$$\frac{\partial^2 \text{Tur}}{\partial {m_\bullet}^2} = \frac{\partial^2 \Gamma}{\partial {m_\bullet}^2} + \frac{\sqrt{d_1 d_2}}{2\left(\det(A_{\text{inh}})\right)^{\frac{3}{2}}} \frac{\partial \det(A_{\text{inh}})}{\partial m_\bullet} - \sqrt{\frac{d_1 d_2}{\det(A_{\text{inh}})}} \frac{\partial^2 \det(A_{\text{inh}})}{\partial {m_\bullet}^2}. \tag{4.38}$$

Lemma 4.3. *The Turing unstable region in $(m_0, \bar{a})$-space becomes smaller as m_{sus} increases.*

Proof. From (4.36) we see that

$$\frac{\partial \det(A_{\text{inh}})}{\partial m_{\text{sus}}} = -\frac{\partial a_2}{\partial m_{\text{sus}}} a_3 = \frac{2n}{1+n^2} n^2 = \frac{2n^3}{1+n^2} > 0,$$
$$\frac{\partial \Gamma}{\partial m_{\text{sus}}} = 0,$$

which together with (4.37) leads to $\frac{\partial \text{Tur}}{\partial m_{\text{sus}}} < 0$, so that the Turing unstable region becomes smaller as m_{sus} increases. □

The range in m_0 for which the Turing instability is not the primary destabilization mechanism may be larger than the lower bound presented in Corollary 4.1, since the increase of m_{sus} pushes the Turing instability to the background (Lemma 4.3) but promotes the Hopf instability (Lemma 4.1). So after the Turing instability emerges from the fold it may still need to overtake the Hopf instability as primary destabilization mechanism, see Figure 4.4.

Natural grazing with $j = 1$

For linear ($j = 1$) natural grazing, it is not as clear how the Turing instability is affected. The component-wise derivative

$$\frac{\partial A_{\text{inh}}}{\partial m_{\text{nat}}} = \begin{pmatrix} 0 & \frac{-2n}{1+n^2} \\ 0 & \frac{n}{1+n^2} \end{pmatrix}. \tag{4.39}$$

of (4.33) yields

$$\begin{aligned}\frac{\partial \det(A_{\text{inh}})}{\partial m_{\text{nat}}} =& a_1 \frac{\partial a_4}{\partial m_{\text{nat}}} - \frac{\partial a_2}{\partial m_{\text{nat}}} a_3 = (-1-n^2)\frac{n}{1+n^2} + \frac{2n}{1+n^2} n^2 \\ =& \frac{n^3-n}{1+n^2} > 0, \\ \frac{\partial \Gamma}{\partial m_{\text{nat}}} =& d_1 \frac{\partial a_{4,\text{inh}}}{\partial m_{\text{nat}}} = \frac{d_1 n}{1+n^2} > 0,\end{aligned} \tag{4.40}$$

and with (4.37) it follows that

$$\begin{aligned}\frac{\partial \text{Tur}}{\partial m_{\text{nat}}} =& \frac{d_1 n}{1+n^2} - \sqrt{\frac{d_1 d_2}{\det(A_{\text{inh}})}} \frac{n^3-n}{1+n^2} \\ =& \frac{\sqrt{d_1 d_2} n}{1+n^2} \left(\sqrt{\frac{d_1}{d_2}} - \frac{n^2-1}{\sqrt{\det(A_{\text{inh}})}} \right),\end{aligned}$$

and when assuming that $m_{\text{sus}} = 0$,

$$\frac{\partial \text{Tur}}{\partial m_{\text{nat}}} = \frac{\sqrt{d_1 d_2} n}{1+n^2} \left(\sqrt{\frac{d_1}{d_2}} - \sqrt{\frac{n^2-1}{m_0 + \frac{m_{\text{nat}}}{1+n^2}}} \right).$$

This implies that the derivative tends to be positive for $n \gtrapprox 1$ but becomes negative for $n \gg 1$. Indeed, it can only be negative if $n^2 > \frac{d_1}{d_2} m_0$, which for $d_1 = 500$, $d_2 = 1$ and $m_0 = 0.45$ (Remark 4.3) leads to $n > 15$ so that through (4.22), $\bar{a} > 6$ is necessary. Thus we conclude that, in this case, for $\bar{a} \leq 6$ the Turing unstable region becomes larger, which is in agreement with Figure 4.4. Together with the monotonicity result Lemma 4.2, this does restrict the Turing instability location for $\bar{a} > 6$.

It is possible to prove a more general result based on the second derivative of Tur with respect to m_{nat}.

Lemma 4.4. *Any region in $(m_0, \bar{a})$-space that becomes Turing unstable due to an increase of m_{nat} will remain unstable as m_{nat} increases further.*

Proof. It holds that

$$\begin{aligned}\frac{\partial^2 \det(A_{\text{inh}})}{\partial {m_{\text{nat}}}^2} =& 0, \\ \frac{\partial^2 \Gamma}{\partial {m_{\text{nat}}}^2} =& 0.\end{aligned}$$

which after substitution together with (4.40) into (4.38) yields $\frac{\partial^2 \text{Tur}}{\partial m_{\text{nat}}^2} > 0$. □

4.5 Simulations with grazing and decreasing rainfall

In this section we show the results of simulations of the extended Klausmeier model (4.15) with grazing incorporated (Section 4.3) to see how the presence of grazing terms changes the desertification process under decreasing rainfall. For this we fix parameters to the values $d_1 = 500$, $d_2 = 1$ and $m_0 = 0.45$ (Remark 4.3). Application of noise tends to decrease the delay in destabilization and the jump in wavenumber at transition [180], in all simulations we apply white multiplicative noise of small amplitude 0.05% (on both the water and the biomass component) at every integer t. Also the rate of change of rainfall a has an influence [180], here we fix $\frac{\partial a}{\partial t} = -10^{-4}$. As initial condition we take the homogeneously vegetated state at a rainfall level where it is still stable. The spatial domain size is 1000, with periodic boundary conditions.

4.5.1 Varying maximum sustained intake

For the simulations presented in this subsection we vary the maximum sustained intake m_{sus} while fixing $I_h = 1$ and $j = 2$. This corresponds to the grazing pressures plotted in Figure 4.5(a). From these plots it is visible that especially for small $I_2(n)$, which encompass patterns with a (very) long wavelength, the grazing pressure becomes exceedingly large. On the other end, from the linear analysis performed in Section 4.4.4 we know that the Turing instability may be delayed (in $\bar{a}$), or even suppressed, by increasing m_{sus} with $j = 2$.

Together with Figure 4.1, the panels in Figure 4.6 show the influence of increasing the maximal intake on the population level (per unit area) m_{sus} on the desertification process driven by decreasing rainfall. We see that the Turing instability occurs at higher values of a, but lower values of $\bar{a} = a - m_{\text{sus}}$, for larger m_{sus}. This is consistent with Lemma 4.3. For the highest value $m_{\text{sus}} = 8$, no Turing patterns form, which is consistent with Figure 4.4 from which it can be read of that, at $m_0 = 0.45$, the Hopf instability occurs at a higher value of $\bar{a}$ (thus also a) than the Turing instability. This is in accordance with main Result 1 of Section 4.1.R

From the simulations it is also visible that for $m_{\text{sus}} \geq 2$, the final transition of the system from a vegetated state to the bare desert state occurs at a relatively small wavelength (large wavenumber) compared to the simulation without grazing (Figure 4.1). This is in supports of main Result 3. In terms

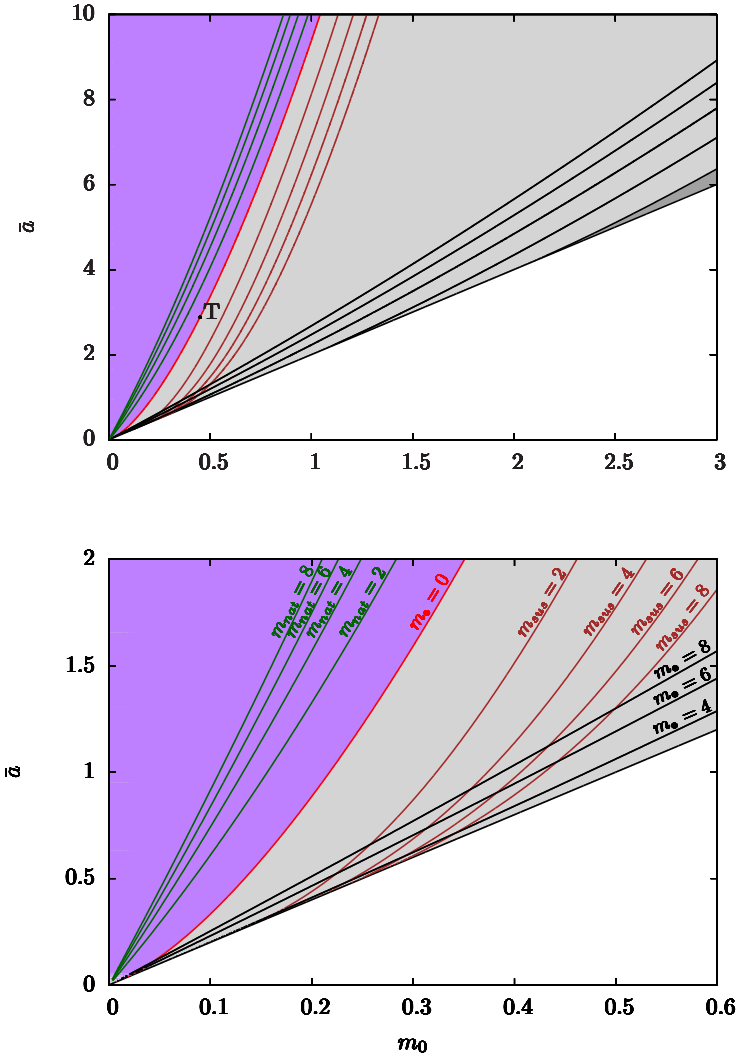

Figure 4.4: The bottom panel is a zoom of the top panel, both showing the influence of grazing on Turing and Hopf instability curves for $d_1 = 500$ and $d_2 = 1$ (Remark 4.3). The red curve is the Turing instability locus without grazing and the purple region is the corresponding Turing stable region. The black line $\bar{a} = 2m_0$, on the boundary of the white region where $(w_\pm, n_\pm)$ does not exist, is the fold bifurcation. Green curves represent Turing instabilities for natural grazing with $j = 1$, $I_h = 1$, L-R: $m_{\text{nat}} = 8, 6, 4, 2$. Brown curves are Turing instabilities for sustained grazing with $j = 2$, $I_h = 1$, L-R: $m_{\text{sus}} = 2, 4, 6, 8$. Black curves show Hopf instability curves, T-B: $m_\bullet = 8, 6, 4, 2, 0$, with $m_\bullet = m_{\text{sus}}$ or m_{nat}. Dark-grey region corresponds to Hopf unstable region in absence of grazing, $m_\bullet = 0$. The point with label T is the locus of the Turing instability for $m_0 = 0.45$, $m_{\text{sus}} = m_{\text{nat}} = 0$.

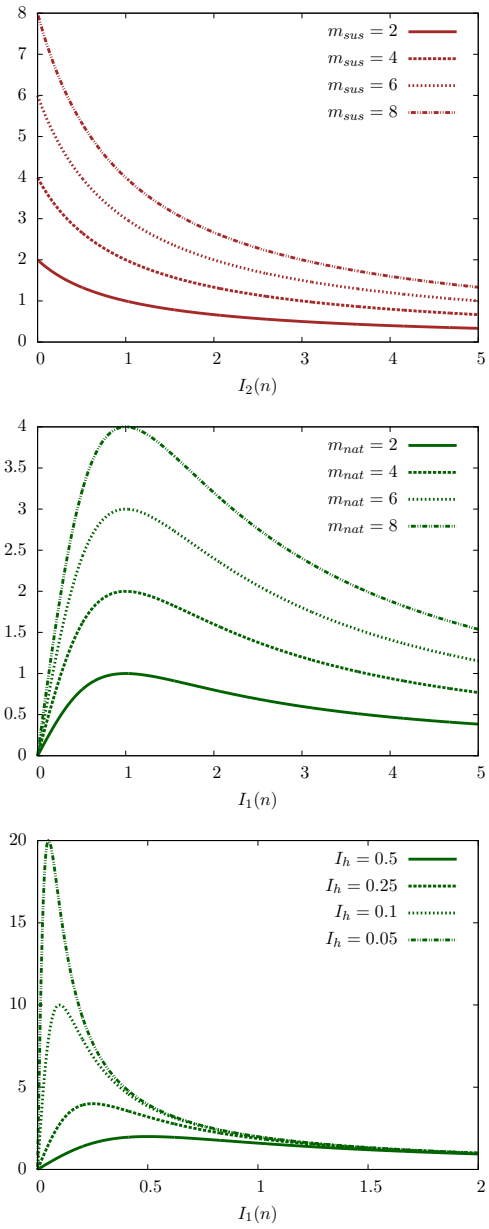

Figure 4.5: Grazing pressures as a function of available forage $I_j(n)$ for the simulations shown in this section. In all cases the grazing pressure monotonically changes for all values of forage. Top panel: sustained grazing with $j = 2$ for $I_h = 1$, varying m_{sus}. Middle panel: natural grazing with $j = 1$ for $I_h = 1$, varying m_{nat}. Bottom panel: natural grazing with $j = 1$ for $m_{\mathrm{nat}} = 2$, varying I_h.

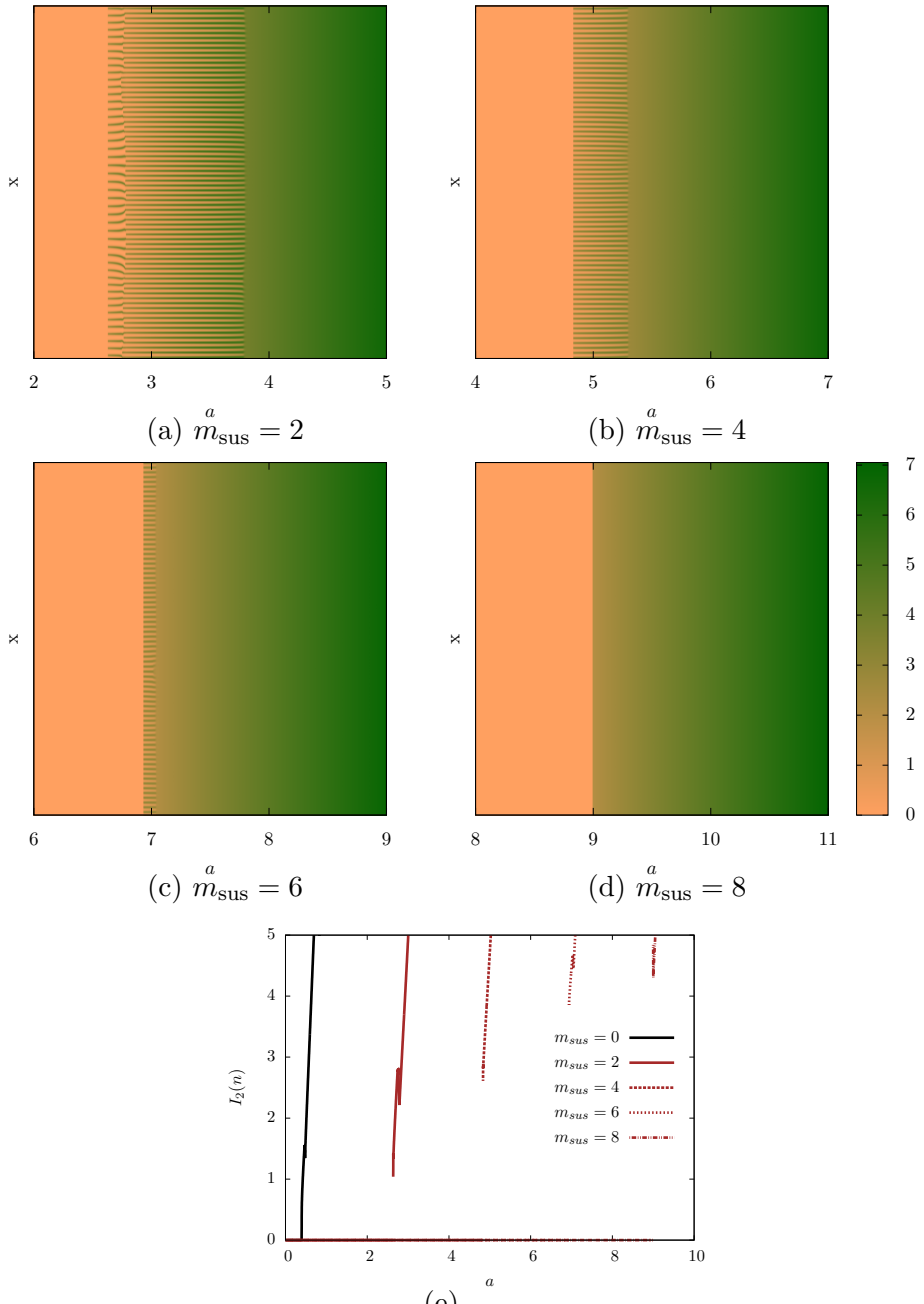

Figure 4.6: Influence of the maximum rate of intake $m_{\text{sus}} = 2, 4, 6, 8$ of sustained grazing with superlinear grazing $j = 2$ on the evolution of vegetation with a slowly decreasing rainfall parameter a, $\frac{\partial a}{\partial t} = -10^{-4}$, and $I_h = 1$. The colorbar besides panel (d) holds for all simulations in this figure. Panel (e) shows the evolution of forage per unit area $I_2(n)$ in the final stages, with very fast jumps to the bare desert state.

of loss of available forage, the final transition to the bare desert state becomes more dramatic as m_{sus} increases, as depicted in Figure 4.6(e) (Result 4, Section 4.1).

4.5.2 Varying maximum natural intake

For the following simulations we vary m_{nat}, while $I_h = 1$ and $j = 1$. Figure 4.5(b) shows that for the simulations shown in this subsection, distributions with $I_1(n) = I_h = 1$ are penalized the most compared to the simulation without grazing in Figure 4.1. This feeds the expectation that transitions from vegetation pattern with large $I_1(n)$ to small $I_1(n)$ occur and the jumps in available forage at these transitions becomes larger as m_{nat} increases. Since in general $g_{j,\text{nat}} \to 0$ as $I_j(n) \to 0$, the destabilization of patterns with low $I_1(n)$ will not occur significantly earlier in a. As a result, the system spends more time residing in vegetation patterns with long wavelength (low wavenumber) as m_{nat} increases, which is confirmed by the simulations in Figure 4.7.

The value of a at the Turing instability, where pattern formation occurs, increases faster than m_{nat} increases. This corresponds to an increasing $\bar{a} = a - m_{\text{nat}}$, which is in line but goes beyond what was shown in Section 4.4.4.

4.5.3 Varying natural herbivore persistence

In the final simulations we vary the herbivore peristence I_h in a natural grazing setting where $m_{\text{nat}} = 2$ and $j = 1$. In Figure 4.5(c) we see that increasing the persistence of herbivores, by decreasing I_h, has a dramatic effect on the grazing pressure on vegetation with small $I_1(n)$ and barely any effect on vegetation with large $I_1(n)$. The panels in Figure 4.8 together with Figure 4.7(a) show how persistence affects the desertification process under decreasing rainfall.

Because we already saw in Figure 4.7(a) that pattern formation at the Turing instability occurs for $n \gg 1$, and persistence does not really affect grazing pressure at this level of available forage $I_j(n)$, it comes as no surprise that the location of the Turing instability in a is not different for different values of I_h (Figure 4.8).

From Figure 4.2(b) we recall that I_h determines at what intermediate value of available forage the grazing pressure is maximal. The smaller I_h,

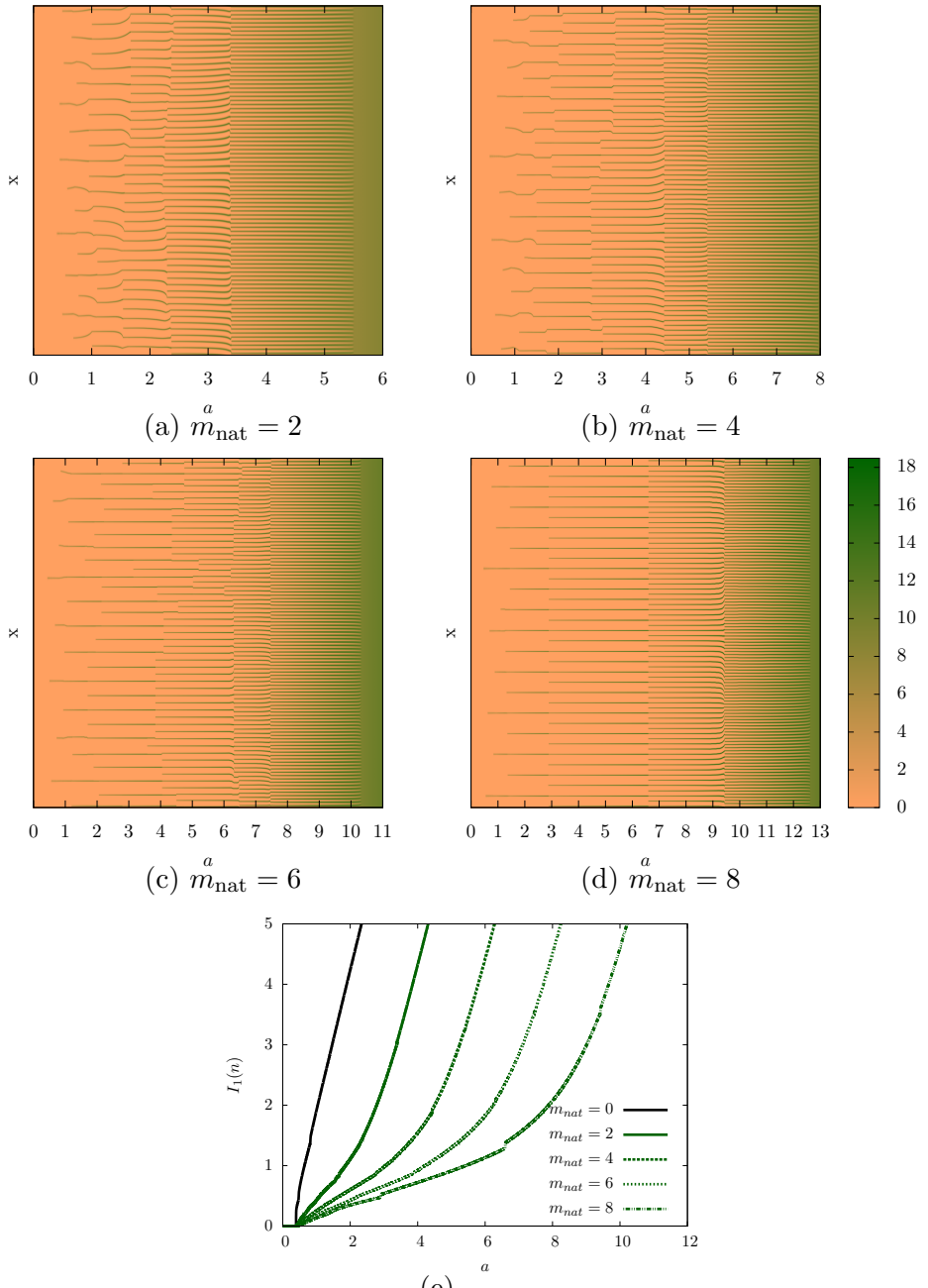

Figure 4.7: Influence of the maximum natural intake of natural grazing $m_{\text{nat}} = 2, 4, 6, 8$ with linear foraging potential ($j = 1$) on vegetation evolution with slowly decreasing rainfall a, $\frac{da}{dt} = -10^{-4}$, and $I_h = 1$. The colorbar besides panel (d) holds for all the simulations in this figure. Panel (e) shows the evolution of forage per unit area $I_1(n)$ in the final stages.

the more dramatic the regime shift from high to low forage is. In Figure 4.8(d), near $a = 3$ a large majority of the vegetation patches disappears, which is also visible as a very fast jump in available forage (Results 3 and 4 of Section 4.1).

Hysteresis is expected to occur when returning from a vegetation pattern with small available forage to a vegetation pattern with large available forage, since intermediate patterns - that the system would reside in on its journey otherwise - are inadmissible. This hysteresis will therefore probably be stronger then reported for systems without explicit grazing [172, 180].

4.6 Discussion and outlook

The effects of grazing on system stability has already been studied for a nonspatial model in [134]. In another nonspatial model [194], soil degradation together with a vegetation dependent herbivore population allows for the possibility of irreversible vegetation change; analysis suggests this is less likely to occur for a natural herbivore population than for human controlled populations. In [196] it is shown that reduced plant cover results in focusing of herbivore grazing on the remaining vegetation, which may lead to the collapse of the entire vegetation [149].

The results in this chapter are in line with these previous model studies. In the simulations (Section 4.5), critical transitions have been shown to occur for both sustained and natural grazing (Result 4). The human controlled case in [196] corresponds to sustained grazing, where the vegetation change leads to the bare desert state, a transition that is irreversible. The prediction of these regime shifts by finding early-warning signals is of great interest [163], e.g. for conservation and management purposes.

We assumed throughout that herbivore dynamics is fast compared to biomass evolution. This assumption may not hold at the very fast transitions in the simulations of Figure 4.8(c) and (d); in that case herbivore population decrease may not keep up with forage decrease, which is expected to lead to an even more dramatic downfall of biomass [178].

We continue by putting forward some promising directions for future analysis and briefly discuss some possible model extensions.

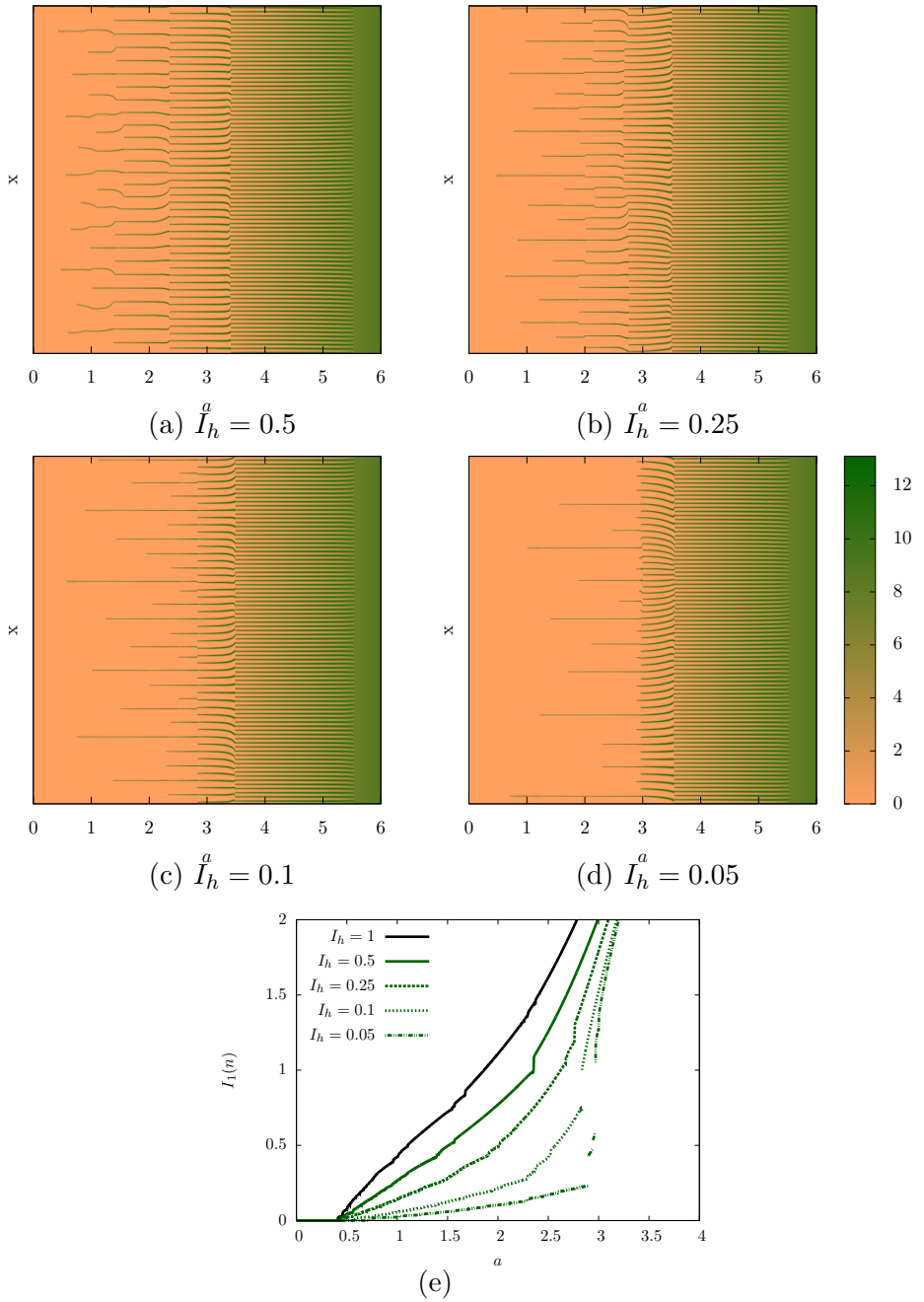

(a) $\overset{a}{I_h} = 0.5$ (b) $\overset{a}{I_h} = 0.25$

(c) $\overset{a}{I_h} = 0.1$ (d) $\overset{a}{I_h} = 0.05$

(e)

Figure 4.8: Influence of the persistence of natural grazing $I_h = 0.5, 0.25, 0.1, 0.05$ with linear foraging potential ($j = 1$) on vegetation evolution with slowly decreasing rainfall a, $\frac{da}{dt} = -10^{-4}$, and $m_{\text{nat}} = 2$. The colorbar besides panel (d) holds for all the simulations in this figure. Panel (e) shows the evolution of forage per unit area $I_1(n)$ in the final stages, with very fast jumps in the regimes with larger persistence.

4.6.1 Analysis

Construction of Busse balloons

Ultimately, the computation of overviews of stable periodic vegetation patterns, called Busse balloons [21, 176, 180, 199], would provide further insight in the influence of grazing on desertification scenarios. A Busse balloon is a representation of stable periodic patterns by a parameter-wavenumber pair. The computation requires the implementation of the linearizations of the grazing terms computed in Appendix 4.A in continuation software.

In this context, we translate the main results from the introduction into the following hypotheses on the Busse balloon.

1. Progressive rate grazing, where $j > 1$, leads to deflation of the Busse balloon.
2. Sustained grazing leads to Busse balloon lift-off. Without grazing the Busse balloon is connected to the x-axis through the existence of stable large wavelength patterns.
3. Natural grazing may split the Busse balloon in two disjoint parts. This may occur if states with intermediate available forage, which become inadmissible due to large grazing pressure, form a connected region in (rainfall, wavenumber)-space.

Concerning hypothesis 1, it would be interesting to see what destabilization mechanism is responsible for the deflation of the Busse balloon. The boundary of the Busse balloon has been found to be given primarily by a sideband instability [180, 199], although for small wavenumbers (large wavelengths) the boundary is given by a Hopf instabilities [51, 199]. Since the destabilization of the homogeneous steady state (w_+, n_+) can become dominated by Hopf instabilities (Section 4.4.4), the same could hold for periodic patterns and a larger part of the boundary of the Busse balloon may consist of Hopf instabilities. In case of a supercritical Hopf instability, the emergence of a limit cycle could act as an early warning signal.

Singular perturbation theory for sustained grazing: obstruction of existence of large wavelength patterns

We briefly sketch how sustained grazing may obstruct the existence of a large wavelength (small wavenumber) patterns, namely that of a single patch, within the extended Klausmeier model (4.15). We start out with the case

$j = 2$.

We view the limit $L \to \infty$, in which the single patch converges to a homoclinic state. In this limit the measure of forage per unit area of the pulse n, $I_2(n)$ (4.4), converges to 0. Thus the grazing pressure $g_{2,\mathrm{sus}}$ (4.8) converges to $\frac{m_{\mathrm{sus}}}{I_h}$. If the loss in vegetation through grazing is larger than the growth through the water uptake,

$$g_{2,\mathrm{sus}} n^2 = \frac{m_{\mathrm{sus}}}{I_h} n^2 > w n^2,$$

then the homoclinic pulse can't be a steady state. Since $w \leq a$ uniformly, it follows that for $a < \frac{m_{\mathrm{sus}}}{I_h}$ the homoclinic pulse does not exist.

For $j = 1$, the nonlocal grazing contributes on the level of the linear death $-m_0 n$. By moving to the homoclinic limit the effective linear death rate becomes $m_0 + \frac{m_{\mathrm{sus}}}{I_h}$.

Much more sophisticated results should be available for both the case $j = 1$ and $j = 2$ by making use of the singular perturbed nature of (4.15), which originates from the fact that $d_1 \gg d_2$. Large wavelength vegetation patterns consist of localized pulses. These pulses can be constructed by using geometric singular perturbation theory [45, 50].

4.6.2 Modeling

Slope and two space dimensions

The analysis here has been restricted to a finite domain in one space dimension without a slope. Future research in two dimensions with downslope water advection could show how grazing affects the stability of vegetation bands [176].

Combination of functional and numerical response

The division between sustained and natural grazing is a division between two extremes. Most populations of herbivores will exhibit both a functional and a numerical response. This may result in a response (4.2) that is the product of a Holling type II functional response and a type III numerical response, again yielding a sigmoid total grazing curve (albeit not of type III).

Palatability

Grazing resistance mechanisms of vegetation include grazing tolerance (large regrowth rates) and grazing avoidance (accessibility and palatability) [40]. In semi-arid rangelands, deterioration of rangelands is shown by replacement of palatable by unpalatable grasses [9]. Experiments confer that selective defoliation of palatable species could lead to their replacement by unpalatable species in grasslands [129]. On a Mongolia study location it was found that sites with a large grazing pressure developed a periodic pattern of unpalatable plants, whereas sites with less grazing pressure have a homogeneous vegetation cover and are dominated by palatable plants [136].

In arid ecosystem modeling it is rather common to make no distinction between plant species with different functional traits, e.g. palatability. It is thus assumed that all the present vegetation is equally available for consumption [134], a notable exception being [69]. A future distinction between palatable and unpalatable vegetation may retrieve the transition from spatially homogeneous predominantly palatable vegetation to an unpalatable periodic vegetation pattern in Mongolia [136]. Also the Holling functional response may change from type II to type III [80], as herbivores may need to learn to distinguish palatable plants in between unpalatable plants.

An increasing percentage of unpalatable vegetation may be an early warning signal for desertification, specific for increased environmental stress due to an increased grazing pressure. Reduced grazing pressure does not promptly lead to the palatable species recovering dominance [204]. The replacement of palatable by unpalatable species is not visible as a collapse in ecosystem biomass, although the economic service provided by the ecosystem does drop dramatically.

4.A General linearization of nonlocal grazing terms

For reference, we compute the linearization of the grazing terms (4.9) and (4.13). These are of use when determining the stability of system states. We start out by linearizing about arbitrary system states and end by simplifying to spatially homogeneous states.

It holds that, for general $j \geq 1$, the *Gâteaux differential* of I_j is given by

$$\begin{aligned} dI_j(n,\tilde{n}) &= \lim_{h\to 0} \frac{I_j(n+h\tilde{n}) - I_j(n)}{h} \\ &= \lim_{h\to 0} \frac{\int_0^L \int_0^1 \frac{d}{ds}(n+hs\tilde{n})^j ds dx}{Lh} \\ &= \lim_{h\to 0} \frac{1}{L}\int_0^L \int_0^1 j(n+hs\tilde{n})^{j-1}\tilde{n}\ ds dx \\ &= \frac{j}{L}\int_0^L n^{j-1}\tilde{n}\ dx \end{aligned} \tag{4.A.1}$$

where we have ignored technical details for interchanging limit and integral.

Now we differentiate $g_{j,\mathrm{sus}}$ and $g_{j,\mathrm{nat}}$:

$$\begin{aligned} dg_{j,\mathrm{sus}}(n,\tilde{n}) &= \lim_{h\to 0} \frac{g_{j,\mathrm{sus}}(n+h\tilde{n}) - g_{j,\mathrm{sus}}(n)}{h} \\ &= \lim_{h\to 0} \frac{\frac{m_{\mathrm{sus}}}{I_h+I_j(n+h\tilde{n})} - \frac{m_{\mathrm{sus}}}{I_h+I_j(n)}}{h} \\ &= \frac{-m_{\mathrm{sus}}}{I_h+I_j(n)} \lim_{h\to 0} \frac{1}{I_h+I_j(n+h\tilde{n})} \frac{I_j(n+h\tilde{n}) - I_j(n)}{h} \\ &= \frac{-m_{\mathrm{sus}}}{(I_h+I_j(n))^2} dI_j(n,\tilde{n}), \end{aligned} \tag{4.A.2}$$

$$\begin{aligned} dg_{j,\mathrm{nat}}(n,\tilde{n}) &= \lim_{h\to 0} \frac{g_{j,\mathrm{nat}}(n+h\tilde{n}) - g_{j,\mathrm{nat}}(n)}{h} \\ &= \lim_{h\to 0} \frac{\frac{m_{\mathrm{nat}} I_j(n+h\tilde{n})}{{I_h}^2+I_j(n+h\tilde{n})^2} - \frac{m_{\mathrm{nat}} I_j(n)}{{I_h}^2+I_j(n)^2}}{h} \\ &= \frac{m_{\mathrm{nat}}}{{I_h}^2+I_j(n)^2} \lim_{h\to 0} \frac{{I_h}^2 - I_j(n)I_j(n+h\tilde{n})}{{I_h}^2+I_j(n+h\tilde{n})^2} \frac{I_j(n+h\tilde{n}) - I_j(n)}{h} \\ &= m_{\mathrm{nat}} \frac{{I_h}^2 - I_j(n)^2}{\left({I_h}^2+I_j(n)^2\right)^2} dI_j(n,\tilde{n}). \end{aligned} \tag{4.A.3}$$

4.A.1 Spatially homogeneous states

Restricting to spatially homogeneous states, denoted by $n_\pm$, the Gâteaux differential of I_j (4.A.1) simplifies to

$$dI_j(n_\pm, \tilde{n}) = \frac{j n_\pm^{j-1}}{L} \int_0^L \tilde{n}\, dx. \tag{4.A.4}$$

Depending on the boundary conditions we can choose an appropriate basis for the perturbations.

Neumann boundary conditions

A basis of $L^2[0, L]$ with Neumann boundary conditions is given by the functions $\tilde{n}_k(x) = \cos(kx)$ with k an integer multiple of $\frac{\pi}{L}$. Substitution in (4.A.4) yields

$$dI_j(n_\pm, \cos(kx)) = \begin{cases} j {n_\pm}^{j-1} & \text{if } k = 0 \\ 0 & \text{if } k \neq 0 \end{cases}$$

Thus the linearization acts differently on spatially homogeneous and spatially inhomogeneous perturbations.

Any perturbation $\tilde{n}$ can be written as a linear combination $\tilde{n} = \sum_{k=0}^{\infty} \beta_k \tilde{n}_k$. Substitution into (4.A.2) and (4.A.3) yields

$$dg_{j,\mathrm{sus}}(n_\pm, \tilde{n}) = \beta_0 \frac{-m_{\mathrm{sus}}}{\left(I_h + {n_\pm}^j\right)^2} j {n_\pm}^{j-1}, \tag{4.A.5}$$

$$dg_{j,\mathrm{nat}}(n_\pm, \tilde{n}) = \beta_0 m_{\mathrm{nat}} \frac{{I_h}^2 - {n_\pm}^{2j}}{\left({I_h}^2 + {n_\pm}^{2j}\right)^2} j {n_\pm}^{j-1}. \tag{4.A.6}$$

Periodic boundary conditions

For periodic boundary conditions a basis is given by functions $\cos(kx)$ and $\sin(kx)$, but now k is an integer multiple of $\frac{2\pi}{L}$, leading to the same results (4.A.5) and (4.A.6) since also $dI_j(n_\pm, \sin(kx))$ vanishes (for k an integer multiple of $\frac{2\pi}{L}$).